

# Efficiency in multiple prediction, leveraging the CMP gather

Matt Eaid and Kris Innanen

## ABSTRACT

Geophysics has seen a shift from mapping large-scale obvious features, to the mapping of subtle features, and accurate inversions for subsurface parameters. The presence of large amplitude multiples in the data makes both of these a challenging task, motivating the need for more robust methods of internal multiple prediction. The most successful method of internal multiple prediction is the fully data-driven algorithm based on the inverse scattering series, which has proven very successful on synthetic data, and is currently being adapted to work on land and marine data. However, one of the main hurdles obstructing its successful application is its computational expense. Typically, computationally expensive 2D algorithms must be applied when the underlying geology contains any structure, in order to produce an accurate prediction. By leveraging properties of the CMP gather we show that the 1.5D algorithm may be applied in the presence of moderate dip, greatly improving efficiency, while maintaining a high level of accuracy.

## INTRODUCTION

Internal multiples continue to pose a significant problem in many geophysical applications. Large amplitude multiples, when they occur in the reservoir have the ability to mask the primary events, obscuring targets, and altering the waveform, making interpretation a challenging task. Additionally, most geophysical processing, and full-waveform inversion algorithms are not designed to handle multiples. The detrimental effect that multiples have on seismic data has motivated substantial research efforts into their removal, with varying degrees of success.

Historically, research into multiple prediction was split into two main camps, those which exploited the periodic nature of multiples, and those which exploited velocity differences between primaries and multiples. Alam and Austin (1981) and Treitel et al. (1982) were among the first to recognize that multiples are exactly periodic in the  $\tau - p$  domain. Application of a sufficiently long deconvolution operator, which searches the data for periodic signals, will predict the multiples in the data set. The large velocity contrast between multiples and primaries, and the resulting moveout difference, saw the development of multiple prediction methods based on stacking out, and FK filtering of multiples (Yilmaz, 2001; Weglein, 1999).

The preceding methods, as well as many others, have seen varying degrees of success in their abilities to accurately predict multiples. However, they all rely on either their assumptions being correct, or some knowledge of subsurface properties. When the underlying assumptions are violated as is usually the case with internal, short period multiples, or accurate knowledge of the subsurface is lacking, most methods of multiple prediction fail. The preeminent method of internal multiple prediction today is one based on the inverse scattering series. The inverse scattering series method of multiple prediction as proposed by Weglein et al. (1997) is a fully data-driven method, that automatically finds all the multiples in the dataset. We begin with a brief overview of the inverse scattering approach to

internal multiple prediction, discuss some of its drawbacks, and propose a remedy to one of those drawbacks by leveraging properties of the common midpoint gather.

## INTERNAL MULTIPLE PREDICTION BASED ON THE INVERSE SCATTERING SERIES

### Internal multiple prediction in 2D

Internal multiple prediction based on the inverse scattering series, proposed by Weglein et al. (1997), utilizes the fact that all internal multiples can be constructed from a triplet of sub-events, provided those sub-events obey a lower-higher-lower relationship. Furthermore every first order internal multiple arrives with a traveltimes that is a combination of the traveltimes of three primaries. Adding the traveltimes of the two deeper (lower) primaries, and subtracting the traveltimes of the shallower (higher) primary gives the exact traveltimes of a multiple. The inverse scattering approach searches through the entire dataset and automatically combines all combinations of events that obey this relationship, automatically predicting all multiples. This is achieved with no underlying assumptions, and the algorithms immense power lies in the fact that it predicts all multiples without any knowledge of the subsurface, meaning it is a fully data-driven algorithm.

Weglein et al. (1997) presented the following 2D algorithm in the wavenumber pseudodepth domain.

$$b_{3IM}(k_g, k_s, \omega) = \frac{1}{(2\pi)^2} \int_{-\infty}^{\infty} \int_{-\infty}^{\infty} e^{-iq_1(\epsilon_g - \epsilon_s)} dk_1 e^{-iq_2(\epsilon_g - \epsilon_s)} dk_2 \times \Psi(k_g, k_1, k_2, k_s | \epsilon) \quad (1)$$

Where,

$$\begin{aligned} \Psi(k_g, k_1, k_2, k_s | \epsilon) = & \int_{-\infty}^{\infty} b_1(k_g, k_1, z) e^{i(q_g + q_1)z} dz \int_{-\infty}^{z-\epsilon} b_1(k_1, k_2, z') e^{-i(q_1 + q_2)z'} dz' \\ & \times \int_{z'+\epsilon}^{\infty} b_1(k_2, k_s, z'') e^{i(q_2 + q_s)z''} dz'' \end{aligned} \quad (2)$$

Equations (1) and (2) combined make up the two dimensional pseudodepth-wavenumber internal multiple prediction algorithm. The vertical wavenumber associated with the source or receiver is given by  $q_x$ , and the total vertical wavenumber is given by  $k_z$ , where each has the following definition,

$$q_x = \frac{\omega}{c_0} \sqrt{1 - \frac{k_x^2 c_0^2}{\omega^2}} \quad (3)$$

and,

$$k_z = q_g + q_s \quad (4)$$

### 2D internal multiple prediction in the coupled planewave domain

Nita and Weglein (2009) and Sun and Innanen (2015) show the relationship,

$$k_z z = \omega t \quad (5)$$

which when substituted into equations (1) and (2) gives the 2D coupled planewave algorithm.

$$b_{3IM}(p_g, p_s, \omega) = \frac{1}{(2\pi)^2} \int_{-\infty}^{\infty} \int_{-\infty}^{\infty} e^{-i\omega(\tau_{1g}-\tau_{1s})} dp_1 e^{-i\omega(\tau_{2g}-\tau_{2s})} dp_2 \times \Psi(p_g, p_1, p_2, p_s|\epsilon) \quad (6)$$

Where,

$$\begin{aligned} \Psi(p_g, p_1, p_2, p_s|\epsilon) = & \int_{-\infty}^{\infty} b_1(p_g, p_1, \tau) e^{i\omega\tau} d\tau \int_{-\infty}^{\tau-\epsilon} b_1(p_1, p_2, \tau') e^{-i\omega\tau'} d\tau' \\ & \times \int_{\tau'+\epsilon}^{\infty} b_1(p_2, p_s, \tau'') e^{i\omega\tau''} d\tau'' \end{aligned} \quad (7)$$

Taken together equations (6) and (7) form the 2D planewave algorithm originally derived by Coates and Weglein (1996), where  $p_s$  and  $p_g$  are the source side and receiver side horizontal slownesses respectively, and where  $\tau$ ,  $\tau'$ , and  $\tau''$  are the intercept times obeying the lower-higher-lower relationship. Where horizontal slowness is defined as,

$$p_x = \frac{\sin \theta_x}{v} \quad (8)$$

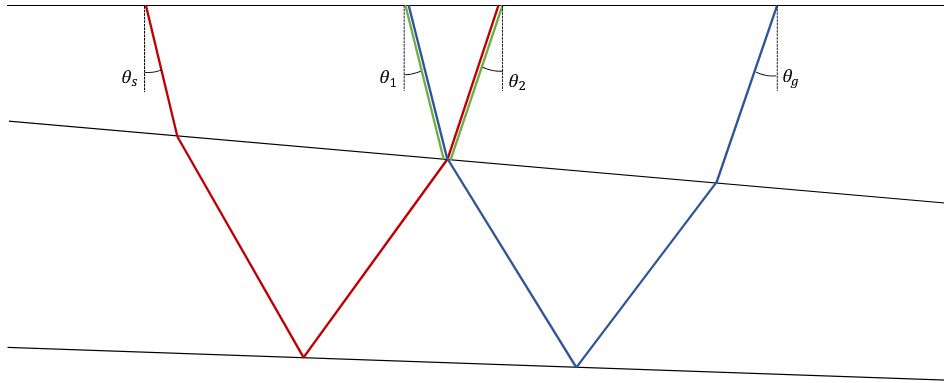


FIG. 1. Ray paths of the sub-event primaries constituting a first order multiple for the 2D case.

Figure 1 shows example subevent primaries that when combined in the 2D planewave algorithm will predict a first order internal multiple. However, the inputs to the 2D plane wave algorithm, namely  $b_1(p_i, p_j, \omega)$ , are not raw prestack shot gathers, but rather prepared coupled slant stack gathers (Sun and Innanen, 2015).

### 1.5 internal multiple prediction in the planewave domain

If the subsurface contains horizontally stratified layers, then by Snell's law  $p_s = p_2$  and  $p_g = p_1$ , implying that  $p_s = p_g$ . It can then be shown that the algorithm in equations (6)

and (7) reduces to (Sun and Innanen, 2014),

$$b_{3IM}(p_g, \omega) = \int_{-\infty}^{\infty} b_1(p_g, \tau) e^{i\omega\tau} d\tau \int_{-\infty}^{\tau-\epsilon} b_1(p_g, \tau') e^{-i\omega\tau'} d\tau' \int_{\tau'+\epsilon}^{\infty} b_1(p_g, \tau'') e^{i\omega\tau''} d\tau'' \quad (9)$$

which is the 1.5D planewave multiple prediction algorithm. Where now the input data is created by slant stacking over receiver side horizontal slowness  $p_g$ .

### Accuracy and efficiency considerations

At the heart of all inverse scattering series prediction algorithms are the search integrals, which for the 2D case are contained in equation (7), and for the 1.5D case lie in equation (9). The search integrals are the integrals which search through the dataset, either in depth, or for the planewave case intercept time, and combine the correct subevents to form all internal multiples in the dataset. The set of three search integrals makes up the bulk of computation time for any given multiple prediction scheme. In the 2D case, because any one  $p_g$  or  $p_s$ , will in general result in many  $p_2$  or  $p_1$  the search integrals run for all possible  $p_1$  and  $p_2$  values, all the while holding  $p_g$  and  $p_s$  constant; which is being handled by the integrals of equation (6). This then must also be repeated for every desired output frequency. The source side and receiver side horizontal slowness are then updated, and the process is repeated for every  $p_g - p_s$  pair. This is a very expensive process as the search integrals are executed many times for a given  $p_g - p_s$  pair, and then this process is repeated many times for each  $p_g - p_s$  pair. Compare this to the 1.5 algorithm, in which the search integrals are repeated once for each output receiver side slowness  $p_g$ , and once for each frequency. This discussion emphasizes that the 2D algorithm is much more computationally expensive than the 1.5D algorithm, so much in fact that currently for large commercial datasets, application of the 2D algorithm is not feasible.

However, as is common in geophysical problems, there is typically a trade off between efficiency and accuracy. When the medium in which our data is acquired from, leads to  $p_g \neq p_s$ , as is the case with dipping strata, then the underlying assumption of the 1.5D algorithm fails, and the algorithm loses accuracy. When the underlying geology is structured we typically must employ the 2D algorithm. Figures 2 and 3 show  $\tau - p$  gathers (a) and a trace extracted from  $p_g \approx 0.3 \times 10^{-4}$  in (b), for the flat and dipping cases respectively. Marked on each trace are the contributing primaries (red "x"), resulting multiple (blue "x"), and the location of the predicted multiple using a 1.5D inverse scattering approach (blue "o"). If the blue "o" overlies the blue "x" then the prediction will be successful. In the case of 1.5D (flat layers) the prediction is successful, however, as expected when the data becomes 2D (dipping layers) as in figure 3, then the prediction loses accuracy.

In general applying 1.5D predictions on 2D data is a fruitless endeavor that results in poor predictions. The following sections will discuss how we can overcome this hurdle, by leveraging properties of the CMP gather, extending the applicability of 1.5D methods, and in turn improving efficiency.

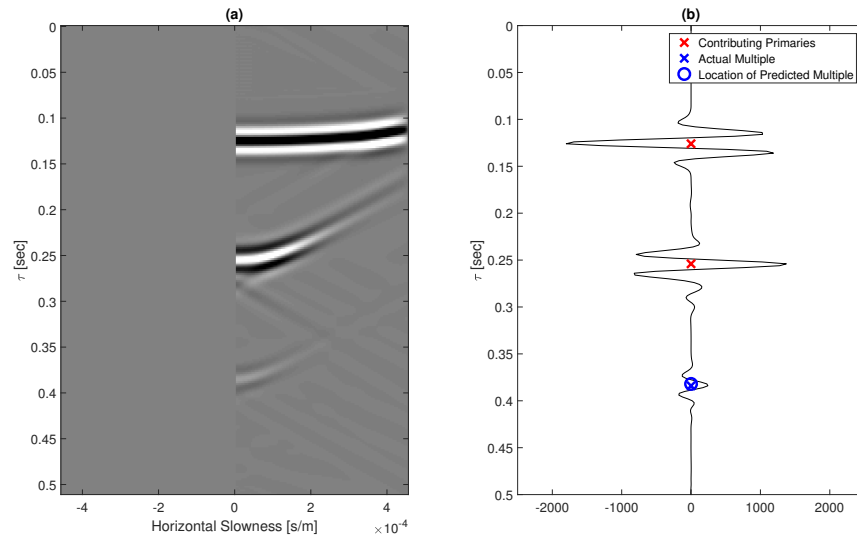


FIG. 2.  $\tau - p$  gather from a model with flat interfaces (a), Trace extracted from  $p_g \approx 0.3 \times 10^{-4}$  (b).

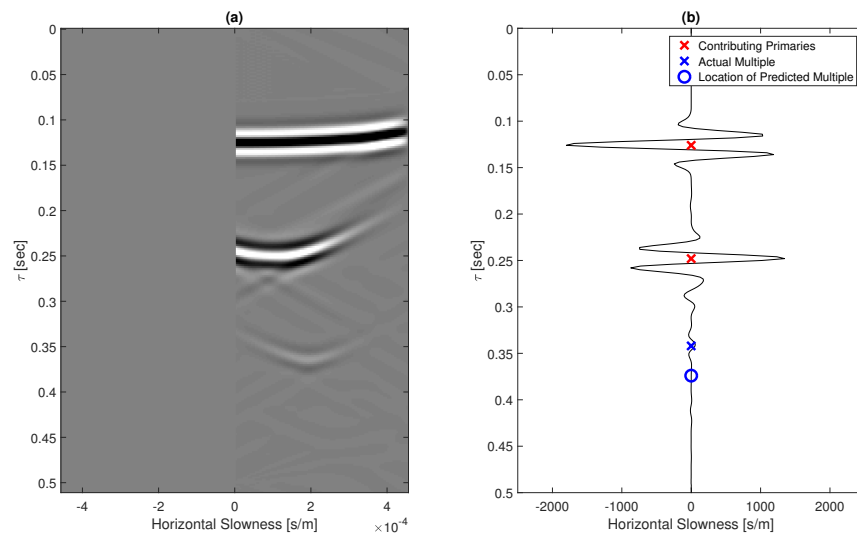


FIG. 3.  $\tau - p$  gather from a model with dipping interfaces (a), Trace extracted from  $p_g \approx 0.3 \times 10^{-4}$  (b).

### THE TRAVELTIME EQUATION IN THE CMP DOMAIN

From our previous discussion, if  $p_g = p_s$  then the more efficient 1.5D prediction algorithm can successfully be applied. In fact, as will be shown, provided that  $p_g \approx p_s$ , the 1.5D algorithm still retains much of its accuracy. By changing the geometry of our experiment, namely by transferring our data from a shot gather geometry, to a common midpoint geometry, we may extend the applicability of the 1.5D algorithm, due to important properties of the CMP geometry. Those properties will now be derived, and their implication on internal multiple prediction will be discussed. As a note, much of the following discussion follows from Diebold and Stoffa (1981).

To start, consider a plane wave propagating in a homogeneous medium, whose direction is governed by the angle with the vertical ( $i$ ).

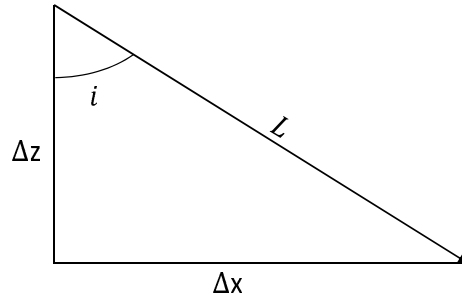


FIG. 4. Schematic diagram of ray propagating in homogeneous media.

Now from figure 4,

$$\Delta x = L \sin(i) = V \Delta T \sin(i) \quad (10a)$$

$$\Delta x \sin(i) = \sin^2(i) V \Delta T \quad (10b)$$

and,

$$\Delta z = L \cos(i) = V \Delta T \cos(i) \quad (11a)$$

$$\Delta z \cos(i) = \cos^2(i) V \Delta T \quad (11b)$$

making use of equations (10a), (10b), (11a), and (11b),

$$\begin{aligned} L^2 &= (V \Delta T)^2 = \Delta x^2 + \Delta z^2 \\ &= (V \Delta T)^2 \sin^2(i) + (V \Delta T)^2 \cos^2(i) \end{aligned}$$

$$V \Delta T = V \Delta T \sin^2(i) + V \Delta T \cos^2(i)$$

$$= \Delta x \sin(i) + \Delta z \cos(i)$$

$$\Delta T = p \Delta x + q \Delta z$$

where,

$$p = \frac{\sin(i)}{V}$$

$$q = \frac{\cos(i)}{V}$$

are the horizontal, and vertical slowness of the ray respectively. If we now consider a medium consisting of horizontally stratified, homogeneous layers, and we integrate along the ray path, the travelttime is,

$$T = px + 2 \sum_j q_j z_j \quad (12)$$

where, the intercept time  $\tau$  is defined as,

$$\tau = T - px = 2 \sum_j q_j z_j \quad (13)$$

The linear moveout equation  $\tau = T - px$  is used in the slant stacking procedure to prepare the 1.5D data.

### Traveltime equation in the presence of dipping interfaces

When we assume flat layers, it can be shown that the horizontal slowness  $p$  is constant along the ray path. This is no longer the case with dipping layers, so now the traveltime equation must be expanded to handle upgoing and downgoing paths separately.

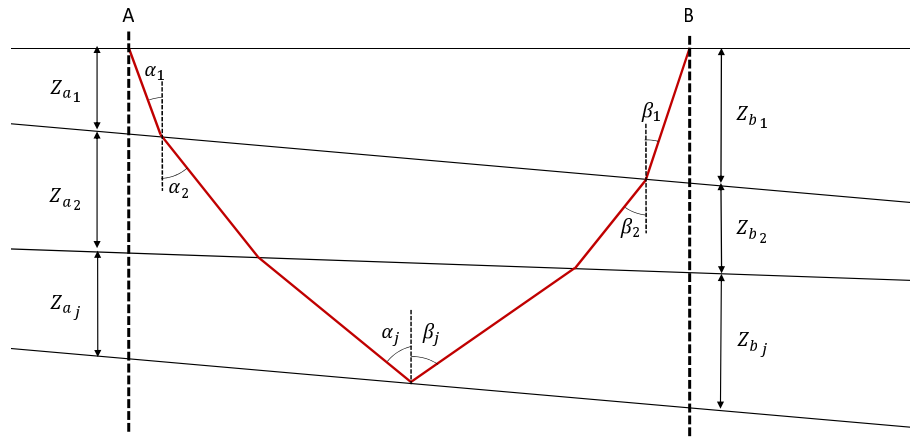


FIG. 5. Geometry for a ray propagating in a medium with an arbitrary number of dipping layers.

Mota (1954) and Ocola (1972) show that for the case of a fixed receiver or source at **A**, that the traveltime of the ray in figure 5 is,

$$T = p_B x + \sum_j Z_{a_j} (q_{a_j} + q_{b_j}) \quad (14)$$

and for a fixed receiver or source at **B**,

$$T = p_A x + \sum_j Z_{b_j} (q_{a_j} + q_{b_j}) \quad (15)$$

The derivation for the case of a fixed source or receiver at **A** is shown in appendix A. When both source and receivers are moving, as is the case in the CMP experiment neither equation (14) or (15) is valid.

In this case, if we draw an arbitrary reference line, as shown by Diebold and Stoffa (1981) we can take a weighted average of equations (14) and (15), as shown in figure 6.

$$\frac{x_A + x_b}{x} = 1 \quad (16a)$$

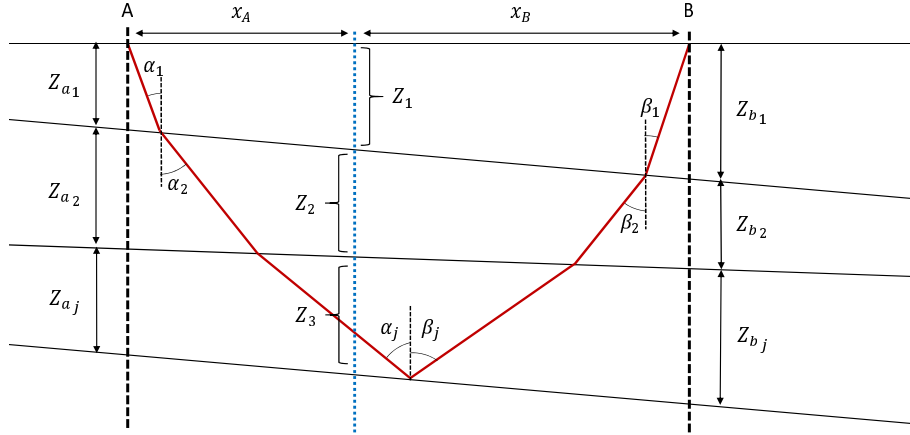


FIG. 6. Geometry for a ray propagating in a medium with an arbitrary number of dipping layers, relative to a reference line.

$$z_j x = x_A z_B + z_A x_B \quad (16b)$$

Since equations (14) and (15) are the traveltimes for the same ray in the same medium, they are equivalent, meaning we can take a weighted average by multiplying them by (16a) and invoke the relationship in (16b).

$$\begin{aligned} T &= \frac{x_A + x_B}{x} (p_B x + \sum_j Z_{a_j} (q_{a_j} + q_{b_j})) \\ &= \frac{x_A (p_B x + \sum_j Z_{a_j} (q_{a_j} + q_{b_j})) + x_B (p_B x + \sum_j Z_{a_j} (q_{a_j} + q_{b_j}))}{x} \\ &= \frac{x_A (p_A x + \sum_j Z_{b_j} (q_{a_j} + q_{b_j})) + x_B (p_B x + \sum_j Z_{a_j} (q_{a_j} + q_{b_j}))}{x} \\ &= \frac{x_A p_A x + x_B p_B x + \sum_j x_A Z_{b_j} (q_{a_j} + q_{b_j}) + \sum_j x_B Z_{a_j} (q_{a_j} + q_{b_j})}{x} \end{aligned}$$

Resulting in,

$$T = x_A p_A + x_B p_B + \sum_j z_j (q_{a_j} + q_{b_j}) \quad (17)$$

Equation (17) is the most general traveltime equation for a ray in dipping strata, and in general is exact for any experimental geometry. In the case of CMP geometry, where  $x_A = x_B = \frac{x}{2}$ , the traveltime for a ray in dipping strata becomes,

$$T = \frac{x}{2} (p_A + p_B) + \sum_j z_j (q_{a_j} + q_{b_j}) \quad (18)$$

which reduces to,

$$T = x \bar{p} + \sum_j z_j (q_{a_j} + q_{b_j}) \quad (19)$$

Equation (19) is the traveltimes for a ray in dipping strata for the special case of the common midpoint geometry. The most important term in equation (19) is  $\bar{p}$  which is an arithmetic average of the source side and receiver side horizontal slowness. The inherent averaging of the source side and receiver side slowness has the result of a marked diminution of dip induced changes in the traveltimes, as we will show, this has profound consequences on internal multiple prediction.

### The impact of common midpoint geometry on internal multiple prediction

Previous discussion indicated that in order for 1.5D prediction algorithms to have success that the relation  $p_g \approx p_s$  must hold. When this relation is not satisfied, as is the case in dipping strata, we typically need to resort to applying 2D prediction algorithms. However, as previously discussed this an undesirable result due to the computational expense of the 2D algorithm.

Equation (19) shows that traveltimes in the CMP geometry depend on an average of the source side and receiver side horizontal slowness. The result of this is a reduction in dip induced changes in the traveltime curves. The secondary result is the fact that even if  $p_g = p_s$  does not hold,  $p_g \approx \bar{p} \approx p_s$  will hold up to some dip. After the dip becomes too large and  $p_g \approx \bar{p} \approx p_s$  no longer holds we will have no choice but to resort to the 2D algorithm, however, the arithmetic averaging of the source and receiver side slowness will extend the applicability of 1.5D algorithms to cases of moderate dip.

Figure 7 (a) shows a  $\tau - p$  gather extracted from a shot record acquired from a model with two layers, where the second layer has a dip of 16 degrees, and figure 7 (b) shows an extracted trace, annotated with the true multiple and where the prediction will try to remove a multiple; it is in fact the same figure as 3. Figure 8 shows the same data, except now the  $\tau - p$  gather has been extracted from a CMP gather. Comparison of figures 7 (b) and 8 (b) shows that the predicted multiple and true multiple are much closer when the prediction is run on the  $\tau - p$  gather extracted from the CMP gather, then on the one extracted from the shot gather. This simple example illustrates that the applicability of the 1.5D prediction algorithm can be greatly extended by applying it to CMP gathers.

## EXAMPLES

The simplest model that will generate internal multiples is one that contains two layers overlying an infinite half space, and as such will be the first one analyzed. Figure 9 shows the velocity model used for testing, the second interface was varied through 0 to 25 degrees of dip in increments of 2 degrees. The 1.5D planewave algorithm was then employed on shot gathers, and CMP gathers from each model to compare the effect of source-receiver geometry on the prediction.

Figures 10 (a), 11 (a), and 12 (a), show split spread shot gathers acquired over the model of figure 9 for dips of 0, 10, and 25 degrees respectively. While 10 (b), 11 (b), and 12 (b), show the resulting predictions. As expected, in the zero dip case where  $p_g = p_s$  is satisfied, the prediction is more or less perfect, and the multiple is removed without harming the primary. As dip progresses from 0 to 10 to 25 degrees, the prediction fails in

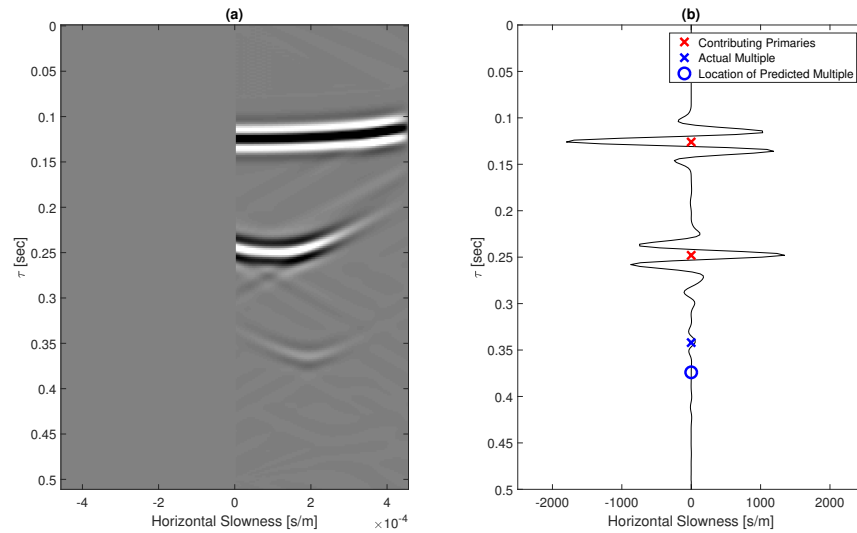


FIG. 7.  $\tau - p$  gather from a shot gather over a model with dipping interfaces (a), Trace extracted from  $p_g \approx 0.3 \times 10^{-4}$  (b).

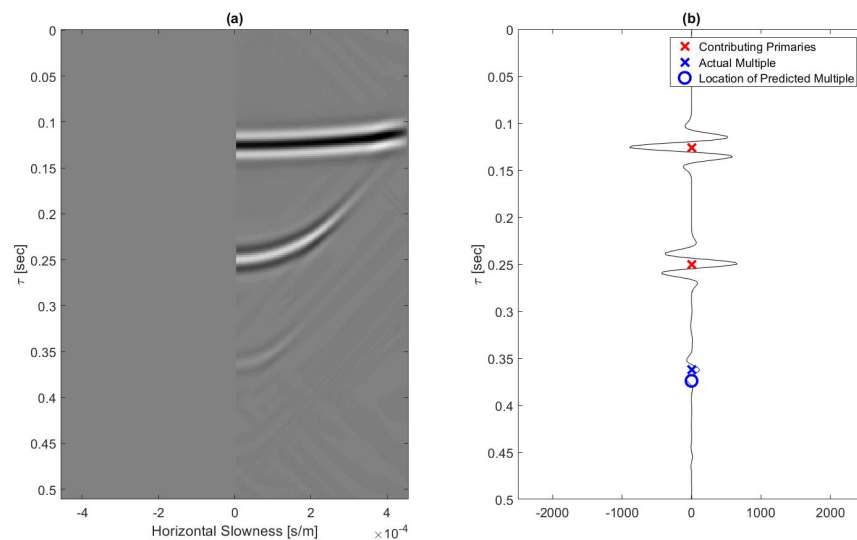


FIG. 8.  $\tau - p$  gather from a CMP gather over a model with dipping interfaces (a), Trace extracted from  $p_g \approx 0.3 \times 10^{-4}$  (b).

its ability to predict a significant portion of the multiple. Figures 13, 14, and 15 show CMP gathers acquired from the same model, as can be seen the prediction is now much more robust in the presence of dip. It is only when the dip becomes severe (around 25 degrees) that the prediction is significantly effected. These results show that in the presence of dip, leveraging properties of the CMP gather leads to a much more robust prediction.

Figure 16 shows the energy removed by the prediction at a given dip, relative to the energy removed in the flat layer case. Assuming that all of the multiple energy was removed in the zero dip case, then a value of one on either curve, indicates that a given prediction was perfect relative to the zero dip case, the smaller a value the worse the prediction was.

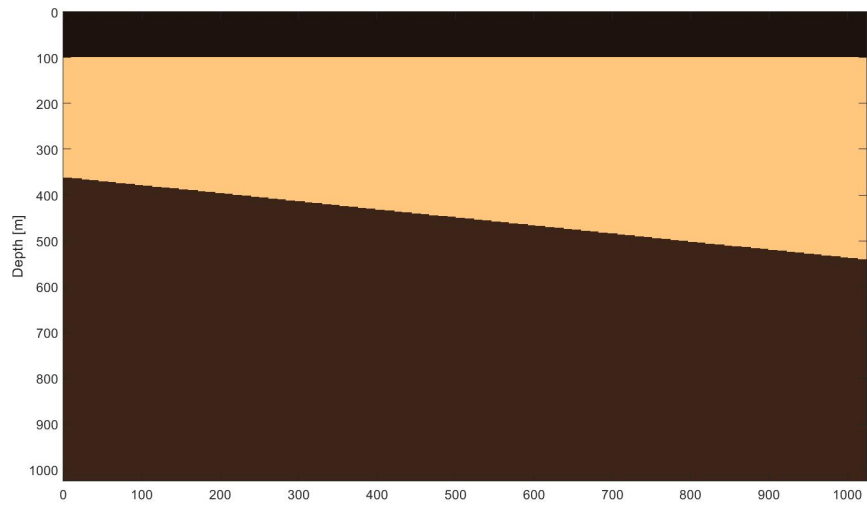


FIG. 9. Velocity model used to generate shots and CMP gathers for multiple prediction.

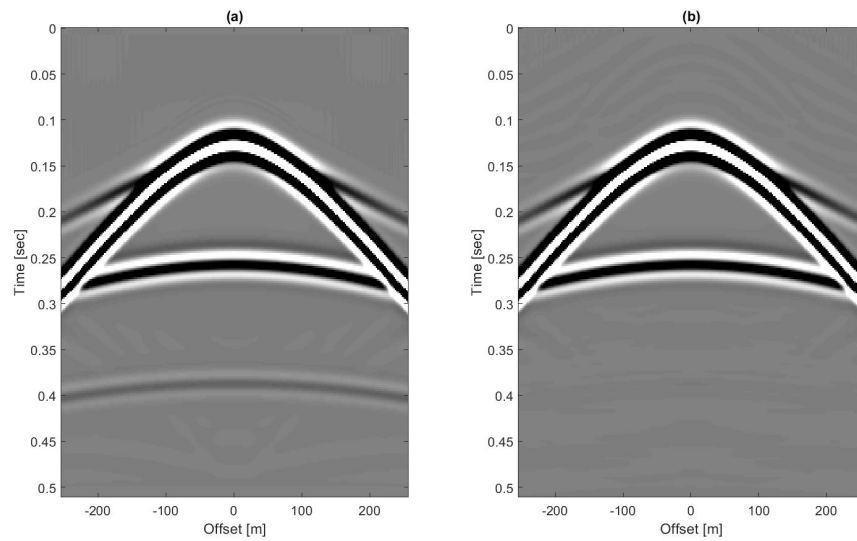


FIG. 10. Shot gather over model with flat layers (a), resulting prediction using the 1.5D planewave prediction scheme (b).

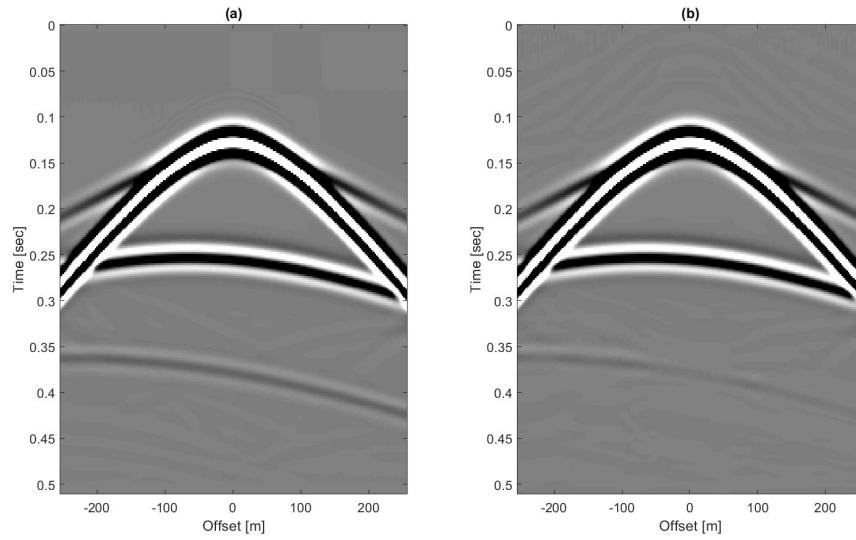


FIG. 11. Shot gather over model with the second layer dipping at 10 degrees (a), resulting prediction using the 1.5D planewave prediction scheme (b).

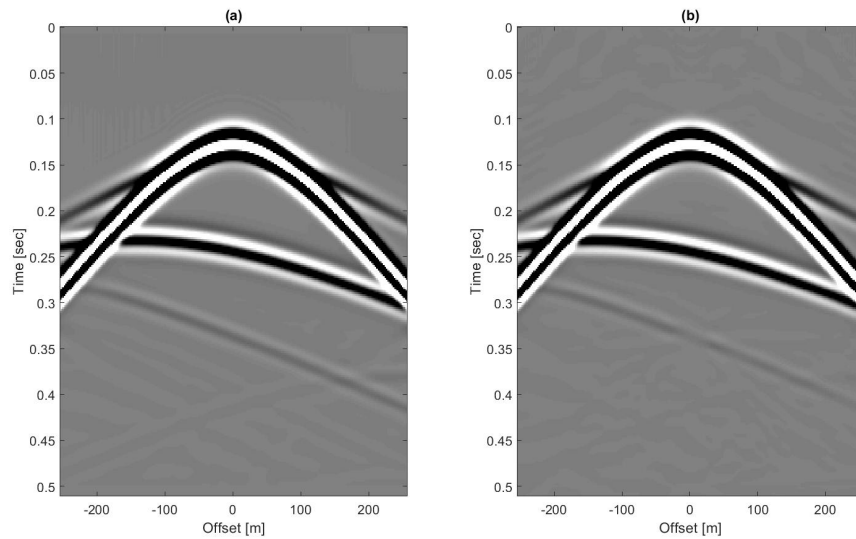


FIG. 12. Shot gather over model with the second layer dipping at 25 degrees (a), resulting prediction using the 1.5D planewave prediction scheme (b).

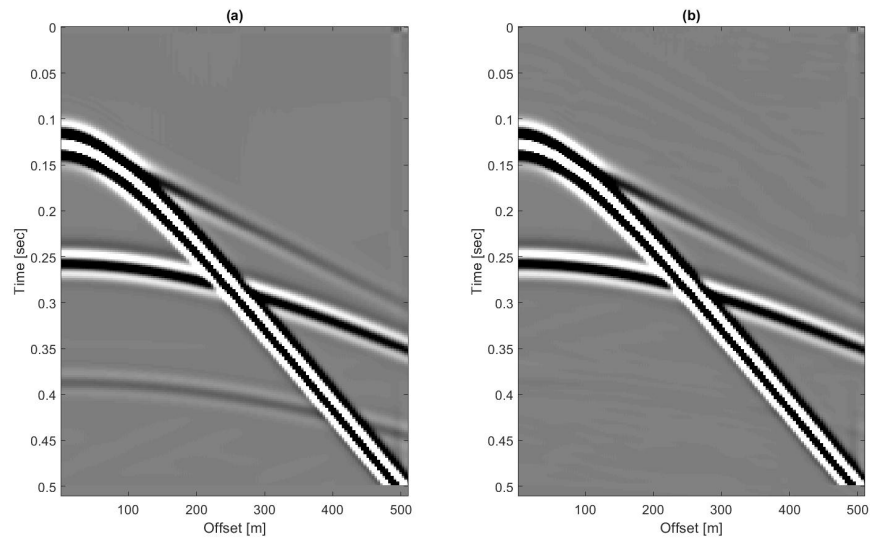


FIG. 13. CMP gather over model with flat layers (a), resulting prediction using the 1.5D planewave prediction scheme (b).

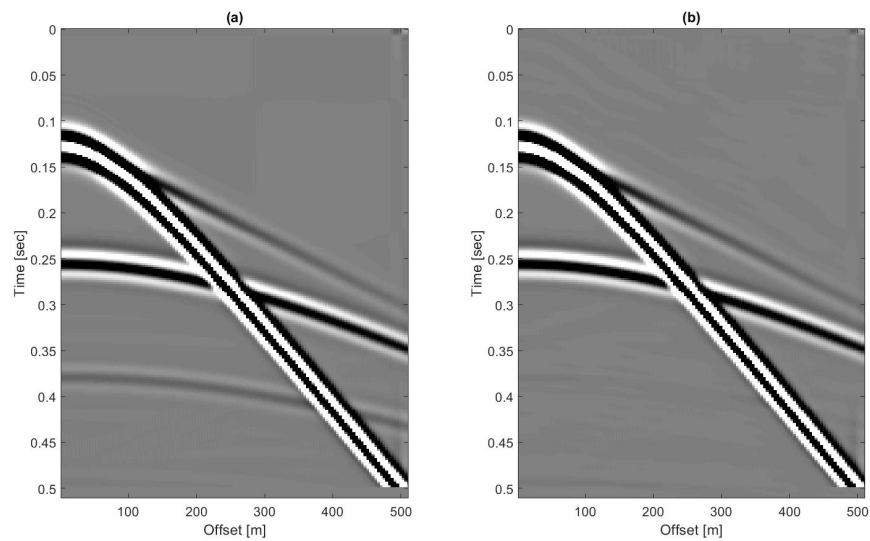


FIG. 14. CMP gather over model with the second layer dipping at 10 degrees (a), resulting prediction using the 1.5D planewave prediction scheme (b).

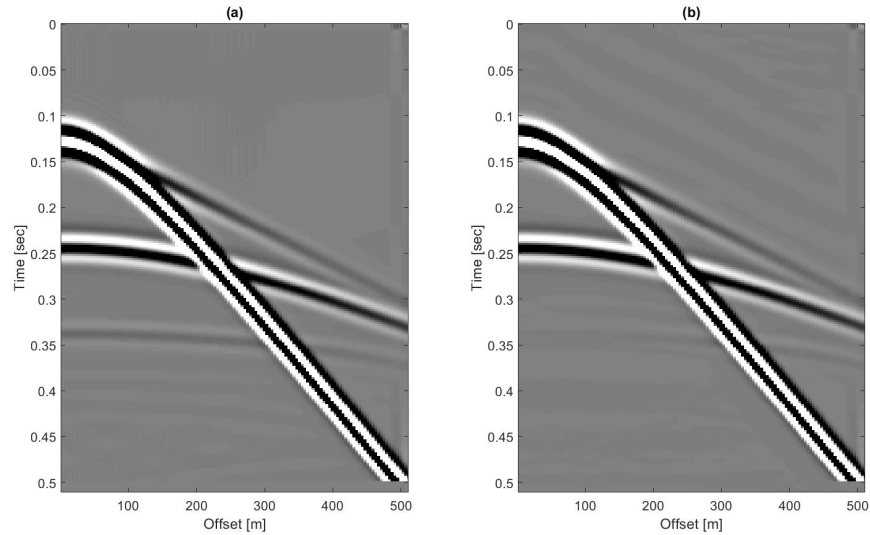


FIG. 15. CMP gather over model with the second layer dipping at 25 degrees (a), resulting prediction using the 1.5D planewave prediction scheme (b).

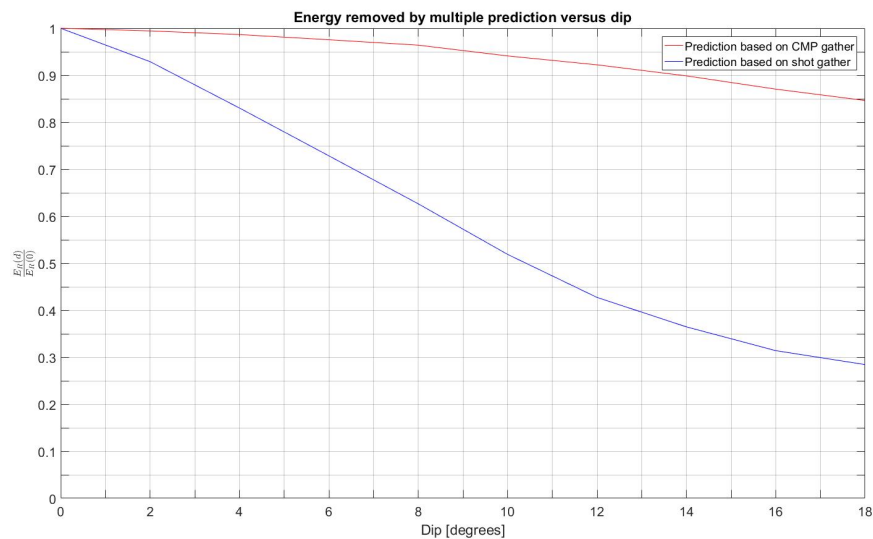


FIG. 16. Energy removed relative to energy removed in the case of a flat reflector versus dip.

In figure 16 the red curve indicates prediction from the CMP gathers, and the blue curve predictions from the shot gathers. Figure 16 clearly shows that the prediction employed on CMP gathers remains much more accurate in the presence of dip.

Although the following examples were encouraging, it is necessary to investigate how these results hold up on more complicated models. Figure 17 shows a velocity model with three dipping interfaces of 2, 4, and 6 degrees respectively. Figure 18 shows a split spread shot gather from the model in figure 17 in (a), and the resulting prediction in (b). Figure 19 shows the same thing as 18 but for a CMP gather. These examples show that in the presence of shallowly dipping layers, the prediction on the shot gather is not very

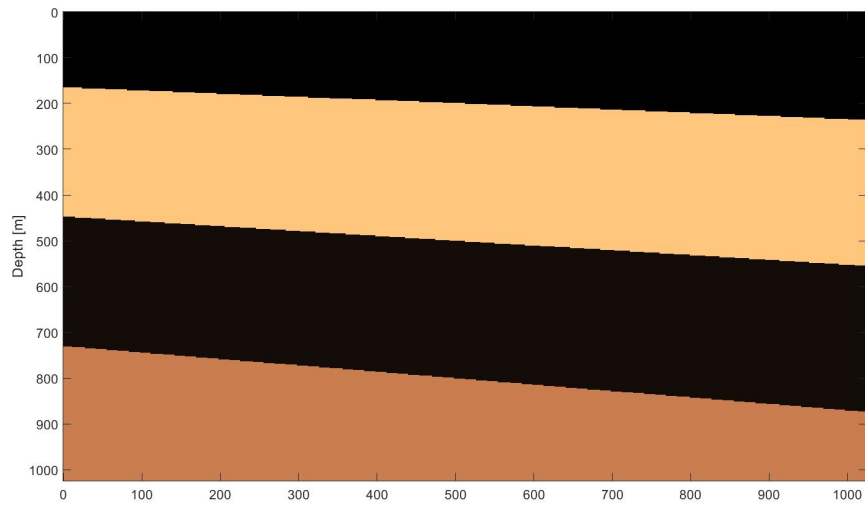


FIG. 17. Velocity model with three dipping interfaces.

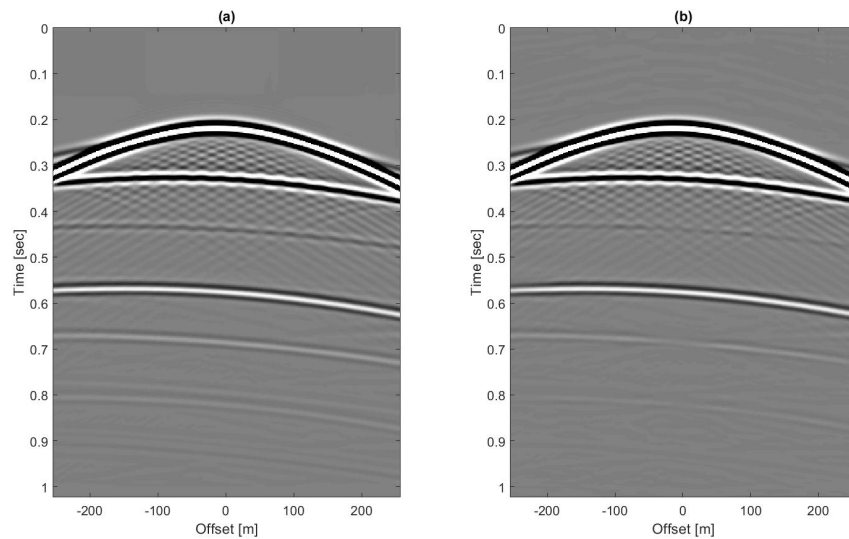


FIG. 18. Shot gather from center of model in figure 17 (a), resulting prediction using the 1.5D planewave prediction scheme (b).

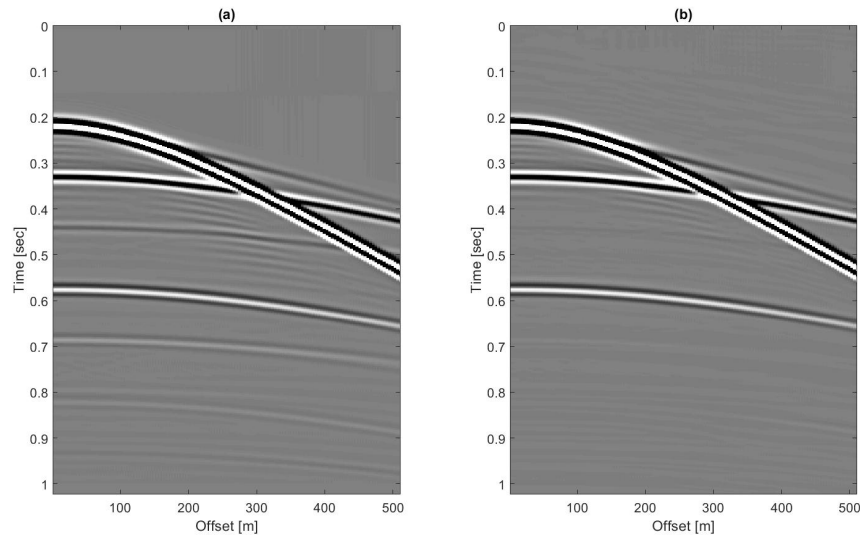


FIG. 19. CMP gather from center of model in figure 17 (a), resulting prediction using the 1.5D planewave prediction scheme (b).

successful, however, the prediction on the CMP gather remains very successful.

## CONCLUSIONS

Typically when a dataset is acquired over 2D geology, if we wish to be successful in predicting all multiples we must apply a full 2D internal multiple prediction based on the inverse scattering series. Unfortunately, this is a very computationally expensive proposition, which is not yet fully realizable on large datasets. We set out with the goal of finding a way of applying the more efficient 1.5D algorithm on data acquired from 2D geology. It was shown that provided the source side and receiver side horizontal slowness were approximately equal ( $p_g \approx p_s$ ) then the 1.5D algorithm could be successfully applied. We then derived the travelttime equation for rays in dipping strata and showed that the travel-time equation for a common midpoint geometry was a function of the average of the source side and receiver side slowness ( $\bar{p}$ ). It was then argued that if  $p_g \approx \bar{p} \approx p_s$  that the 1.5D algorithm could be successfully applied to CMP gathers from 2D (dipping) geology. Examples showed that predictions from shot gathers over dipping strata lost accuracy relatively rapidly as the dip increased, however, the predictions from the CMP gathers maintained a high level of accuracy even in the presence of large dip.

## ACKNOWLEDGMENTS

The authors would like to thank the sponsors of the CREWES project as well NSERC under the grant CRDPJ 461179-13 for making this work possible through their financial support.

## REFERENCES

- Alam, A., and Austin, J., 1981, Multiple attenuation using slant stacks: Technical Report, Western Geophysical Company.
- Coates, R., and Weglein, A., 1996, Internal multiple attenuation using inverse scattering: results from prestack 1 and 2d acoustic and elastic synthetics: SEG Expanded Abstracts, 1522–1525.
- Diebold, J., and Stoffa, P., 1981, The traveltine equation, tau-p mapping, and inversion of common midpoint data: *Geophysics*, **46**, No. 3, 238–254.
- Mota, L., 1954, Determination of dips and depths of geological layers by the seismic refraction method: *Geophysics*, **19**, 242–254.
- Nita, B., and Weglein, A., 2009, Pseudo-depth/intercept-time monotonicity requirements in the inverse scattering algorithm for predicting internal multiple reflections: *Communications in Computational Physics*, **5**, 163–182.
- Ocola, L., 1972, A nonlinear least-squares method for seismic refraction mapping - part 2: model studies: *Geophysics*, **37**, 273–287.
- Sun, J., and Innanen, K., 2014, 1.5D internal multiple prediction in the plane wave domain: CREWES Research Reports, **26**, No. 74.
- Sun, J., and Innanen, K., 2015, 2D internal multiple prediction in coupled plane wave domain: CREWES Research Reports, **27**, No. 69.
- Treitel, S., Gutowski, P., and Wagner, D., 1982, Plane wave decomposition of seismograms: *Geophysics*, **47**, 1372–1401.
- Weglein, A., 1999, Multiple attenuation: an overview of recent advances and the road ahead: *The Leading Edge*, **18**, No. 1, 40–44.
- Weglein, A., Gasparotto, F., Carvalho, P., and Stolt, R., 1997, An inverse-scattering series method for attenuating multiples in seismic reflection data: *Geophysics*, **62**, 1975–1989.
- Yilmaz, O., 2001, *Seismic Data Analysis*: Society of Exploration Geophysicists.

## APPENDIX A: TRAVELTIME EQUATION FOR A RAY IN DIPPING MEDIA

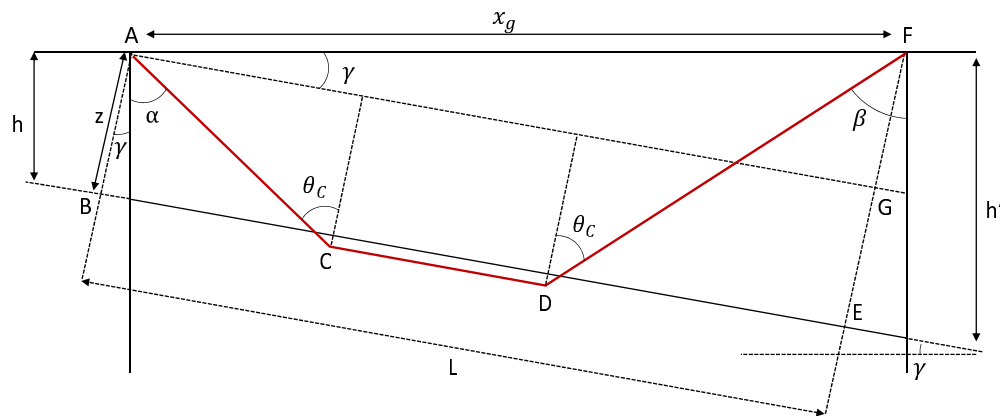


FIG. 20. Geometry for critically refracted ray in medium with dipping strata.

$$T_{AF} = \frac{AC}{v_0} + \frac{CD}{v_1} + \frac{DF}{v_0} = \frac{AC + DF}{v_0} + \frac{CD}{v_1}$$

Using the relation that  $CD = L - BC - DE$ ,

$$T_{AF} = \frac{AC + DF}{v_0} + \frac{L - BC - DE}{v_1}$$

Making the substitutions  $L = x_g \cos \gamma$ ,  $AB \cdot \tan \theta_c = BC$ , and  $EF \cdot \tan \theta_c = DE$ .

$$T_{AF} = \frac{AB + EF}{v_0 \cos \theta_c} + \frac{x_g \cos \gamma - \tan \theta_c (AB + EF)}{v_1}$$

Collecting like terms and subbing in the appropriate trigonometric form of  $\tan \theta_c$ .

$$T_{AF} = \frac{x_g \cos \gamma}{v_1} + (AB + EF) \left[ \frac{1}{v_0 \cos \theta_c} - \frac{\sin \theta_c}{v_1 \cos \theta_c} \right]$$

Pulling out the common denominator, and using Snell's law to substitute for  $\sin \theta_c$ .

$$T_{AF} = \frac{x_g \cos \gamma}{v_1} + \frac{(AB + EF)}{v_0 \cos \theta_c} \left[ 1 - \left( \frac{v_0}{v_1} \right)^2 \right]$$

Using the relations,  $\sin \theta_c = \frac{v_0}{v_1}$ , and  $\cos^2 \theta = 1 - \sin^2 \theta$

$$T_{AF} = \frac{x_g \cos \gamma}{v_1} + \frac{(AB + EF) \cos \theta_c}{v_0}$$

Making use of  $EF = x_g \sin \gamma + AB$ , and  $\frac{\sin \theta_c}{v_0} = \frac{1}{v_1}$ .

$$T_{AF} = \frac{x_g \cos \gamma \sin \theta_c}{v_0} + \frac{(AB + AB + x_g \sin \gamma) \cos \theta_c}{v_0}$$

$$T_{AF} = \frac{x_g}{v_0} (\cos \gamma \sin \theta_c + \sin \gamma \cos \theta_c) + 2 \frac{AB}{v_0} \cos \theta_c$$

Now using the trig identity  $\sin(A \pm B) = \sin A \cos B \pm \cos A \sin B$ .

$$T_{AF} = \frac{x_g}{v_0} \sin(\gamma + \theta_c) + 2 \frac{z \cos \theta_c}{v_0}$$

Using  $\beta = \gamma + \theta_c$ , in conjunction with  $z = h \cdot \cos \gamma$ .

$$T_{AF} = \frac{x_g}{v_0} \sin \beta + \frac{2h \cos \gamma \cos \theta_c}{v_0}$$

Now making use of the relations  $p_B = \frac{\sin \beta}{v_0}$ , and  $\cos A \cos B = \cos(A - B) + \cos(A + B)$ .

$$T_{AF} = x_g p_B + \frac{h [\cos(\gamma - \theta_c) + \cos(\gamma + \theta_c)]}{v_0}$$

Finally using,  $\alpha = \gamma - \theta_c$ ,  $\beta = \gamma + \theta_c$ , and  $q_A = \frac{\cos \alpha}{v_0}$ ,  $q_B = \frac{\cos \beta}{v_0}$ .

$$T_{AF} = x_g p_B + \frac{h}{v_0} [\cos \alpha + \cos \beta]$$

$$T_{AF} = x_g p_B + h(q_A + q_B)$$

Intuitively this may be extended to many interfaces giving us the result in equation (14).

$$T = p_b x + \sum_j h_j (q_{a_j} + q_{b_j})$$